First-principles study of the solubility, diffusion, and clustering of C in Ni

Donald J. Siegel* and J. C. Hamilton
Sandia National Laboratories, Mail Stop 9161, Livermore, California 94551, USA
(Received 2 April 2003; revised manuscript received 17 June 2003; published 4 September 2003)

Within the framework of density functional theory, we investigate three key properties of a C interstitial solid solution in crystalline Ni: the heat of solution (ΔH_{sol}), the activation energy for C diffusion (E_a), and the C-C pair binding energy (B). In addition, we assess the impact of Ni magnetism upon each property. The most energetically favorable lattice site for C is the interstitial octahedral site (O site), which is 1.59 eV lower in energy than the tetrahedral site (T site). Using the nudged elastic band method, we determine that diffusion between O sites proceeds via a T-site intermediate. The calculated activation energy ($E_a = 1.62$ eV), is in good agreement with experimental data from the literature (1.54–1.71 eV). The binding of C pairs is sensitive to magnetization effects, and is negligible ($B \approx 0$ eV) in the ferromagnetic state, but repulsive in the paramagnetic state ($B = -0.2$ eV). These results are consistent with anelastic relaxation experiments, which find $B < 0.1$ eV in the FM state. The calculated heat of solution in the paramagnetic Ni state ($\Delta H_{\mathrm{sol}}^{\mathrm{para}} = 0.2$–$0.35$ eV) is in reasonable agreement with high-temperature experimental values of ~ 0.4 eV, and the magnitude of ΔH_{sol} in the ferromagnetic state is found to be about 0.4 eV greater than in the paramagnetic state. Lastly, we briefly assess the effect of pseudopotential choice and exchange-correlation functionals upon the accuracy of the results.

DOI: 10.1103/PhysRevB.68.094105 PACS number(s): 61.72.Ji, 66.30.Jt, 71.15.Mb, 75.50.Bb

I. INTRODUCTION

Carbon is commonly present in the iron-group transition metals (Fe, Co, Ni) either as an impurity or as an alloying agent. As the solute in a solid solution, C occupies interstitial sites due to its relatively small atomic size,[1] and has been studied extensively because of its impact on the microstructural stability and mechanical properties of austenitic steels. More recently, and at a much smaller length scale, electrodeposited Ni-C alloys have been proposed for use as components in microelectromechanical systems (MEMS). In this case C enters via additives to the electrolyte solution, which act as nucleation agents for grain growth.[2]

The fundamental properties of the Ni-C system have been the subject of several experimental studies. The high-temperature solubility (i.e., at temperatures a few hundred degrees above the Curie point $T_c = 627$ K,) has been studied by at least three groups,[3–5] wherein Arrhenius plots of the C concentration vs inverse temperature yielded heats of solution (ΔH_{sol}) with respect to graphite in the range of 0.42–0.49 eV. The most likely location for C in the Ni FCC lattice is believed to be at octahedral interstitial sites; however, the energetics of other possible sites have yet to be examined. It is notable that in some related systems (such as Ni-H and NiCo-C) there have been reports of abrupt changes in solute ΔH_{sol} at T_c.[6,7] Herein we briefly revisit this issue, which was the focus of a more detailed prior investigation.[8]

The diffusion of C in Ni has also been studied using a variety of techniques,[1,4,9–12] both above[4,9,10,12] and below[1,11] T_c. At high temperatures, diffusion is attributed to the migration of isolated C atoms. Measured activation energies (E_a) range from 1.54 to 1.71 eV. The mechanism of diffusion, however, is unknown. Because Ni has a relatively low Curie point, direct measurements of the diffusion of isolated C for $T < T_c$ are impractical due to the long time scales involved. Low-temperature experiments, therefore, rely on the anelasticity of C pairs, in which the activation energy for diffusion is attributed to the reorientation of a pair. Along these lines, Diamond and Wert[11] used several techniques to study C pair relaxation both above and below T_c; they determined that the effect on the diffusivity of the magnetic transition was negligibly small, and that the activation energy for the relaxation of 1.51 eV was in good agreement with the high-temperature data previously reported by others. Using similar techniques, a more recent experiment by Numakura and co-workers[1] attempted to measure the C-C pair binding energy (i.e., clustering tendency B), and in so doing estimate the overall pair concentration. They concluded that the binding was small, and probably less than 0.1 eV. Since density functional simulations can directly evaluate the binding energy, we do so below for a few candidate C pair configurations.

Another topic of interest is the mechanisms by which interstitial atoms diffuse in polycrystalline materials by way of grain boundaries (GB's). By first examining the properties of the bulk Ni-C system, we lay the groundwork for a future study of GB diffusion and facilitate comparisons between diffusion in the two regimes. Furthermore, a rich experimental database exists for the bulk Ni-C system against which we can critically assess the accuracy of our density-functional methods and determine the impact of computational parameters such as pseudopotential choice, spin polarization, and exchange correlation functionals. The large supercell sizes needed for grain boundary studies, and a relative dearth of specific experimental GB data for Ni-C, make testing on that system less advantageous.

In addition to providing a careful comparison between theory and experiment regarding ΔH_{sol}, E_a, and B for Ni-C, our calculations also aim to address some of the outstanding issues which are more difficult to examine experimentally. These include: the impact of Ni ferromagnetism upon ΔH_{sol},

E_a, and B; the optimal C interstitial site; the mechanisms and respective E_a's for C diffusion; and B's for a few C-C pair configurations.

II. METHODOLOGY

Our density functional[13,14] calculations were performed with the VASP,[15] code which uses a planewave basis set for expansion of the electronic wavefunctions, and pseudopotentials[16–18] to describe the computationally expensive core-valence interaction. Brillouin zone sampling was performed using a Monkhorst-Pack grid[19] of special **k** points, and electronic occupancies were determined according to a Methfessel-Paxton scheme[20] with an energy smearing of 0.1 eV. Independent **k**-point convergence tests were conducted for each distinct supercell geometry, ranging from the primitive cell of bulk Ni up to the largest 109-atom cells used for C clustering calculations. For the majority of this study we used the generalized gradient approximation (GGA) of Perdew and co-workers[21] (PW91) for the exchange-correlation energy; however, for most properties we also performed comparison calculations using the local density approximation (LDA).[14,22,23] For pseudopotentials (pp) we choose between two sets: the first is based on the ultrasoft (US) scheme devised by Vanderbilt,[16,17] which takes the $4s$ $3d$ states as the valence configuration for Ni. The second set uses Blöchl's all-electron-like projector augmented wave method (PAW),[18,24] and additionally includes the $3p$ semicore states as Ni valence. Planewave convergence testing on these two sets was performed using a four-atom Ni conventional cell with a C atom at an octahedral interstitial site. While the US set required a cutoff of only 290 eV to obtain a 1 meV convergence in total energy/atom, a cutoff of up to 700 eV was necessary for the much ''harder'' PAW set. The exchange-correlation functionals utilized in the atomic calculations for generation of the pseudopotentials were consistent with the functionals used in the present Ni-C calculations. That is, pp's generated within the LDA were used only in LDA-based Ni-C calculations, and likewise for the GGA.

As a first test of our methods we calculated the properties of bulk Ni in order to evaluate three parameters—pseudopotential choice, exchange-correlation functionals, spin polarization effects—and to compare with other experimental and theoretical results. Using the primitive cell geometry, 60 irreducible **k** points and a planewave cutoff energy of 260 eV (400 eV for the PAW) were needed to converge the total energy per atom to within 1 meV. Results for the lattice constant (a), bulk modulus (B_0), magnetic moment (μ_B), and cohesive energy (E_{coh}) are compiled in Table I, and show that of the three factors in question, the one which is of the most significance is the exchange-correlation functional: the GGA gives substantially better agreement with experiment than the LDA in terms of a, B_0, and E_{coh}, and also yields slightly better values for μ_B. The inclusion of spin polarization or use of PAW vs ultrasoft pseudopotentials has only a minor impact. We also note that our results are consistent with other *ab initio* LAPW (Ref. 25) and all-electron[26] calculations. We will further investigate the importance of spin polarization and pseudopotential choice on the Ni-C system in the following sections.

TABLE I. Comparison of calculated Ni properties to experiment and other *ab initio* calculations. LDSA refers to spin-polarized LDA calculations and GGS refers to spin-polarized GGA calculations.

Method	a (Å)	B_0 (GPa)	M_0 (μ_B)	E_{coh} (eV)
US-LDA	3.430	260		6.06
US-LSDA	3.435	250	0.58	6.10
PAW-LDA	3.421	258		6.09
PAW-LSDA	3.427	253	0.58	6.13
LSDA, PP-LAPW [a]	3.44	239	0.60	
US-GGA	3.525	195		4.87
US-GGS	3.533	199	0.62	4.93
PAW-GGA	3.516	202		4.87
PAW-GGS	3.522	196	0.60	4.93
GGS, PP-LAPW [a]	3.53	192	0.64	
FLAPW–GGS [b]	3.52	200	0.60	
Experiment [c]	3.52	186	0.61	4.44

[a]Reference 25.
[b]Reference 26.
[c]Reference 27.

III. HEAT OF SOLUTION

In the fcc Ni lattice there are two high-symmetry interstitial sites available for C occupation: the octahedral (O) site [conventional cell coordinates $(\frac{1}{2},\frac{1}{2},\frac{1}{2})$] [see Fig. 4(a)], and the tetrahedral (T) site [coordinates $(\frac{1}{4},\frac{1}{4},\frac{1}{4})$] [Fig. 4(d)]. We investigated both positions using the US pp set (initially), with a supercell constructed from a $2\times2\times2$ replication of the conventional Ni unit cell, resulting in a total of 33 atoms and a C concentration of 3.03%. Earlier reports[28,29] on ΔH_{sol} of impurities in Al and Mg have shown that careful **k**-point sampling was necessary to obtain converged results. Our own tests of **k**-point convergence and supercell-size effects revealed that a 33 atom cell using 10 **k** points gave ΔH_{sol} values converged to 0.02 eV with respect to calculations using 20 **k** points or a 65-atom supercell (see Table II). Both the internal atomic coordinates and the magnitude of the supercell lattice vectors were optimized by performing a series of constant volume calculations in which the atomic coordinates for each volume were relaxed to a force tolerance of 0.05 eV/Å per atom. This energy vs. volume data was then fit to the Murnaghan equation of state[30] to obtain the optimal geometry/minimum energy configuration.

The heat of solution of C in Ni with respect to graphite was calculated for each site according to the formula

$$\Delta H_{\mathrm{sol}} = E_{\mathrm{tot}}(\mathrm{Ni+C}) - [E_{\mathrm{tot}}(\mathrm{Ni}) + \mu_{\mathrm{C}}], \tag{1}$$

where $E_{\mathrm{tot}}(\mathrm{Ni+C})$ is the total energy of the interstitial Ni+C system, $E_{\mathrm{tot}}(\mathrm{Ni})$ is the energy of the 32-atom Ni cell without C, and μ_{C} is the energy per C atom in graphite. To minimize errors, $E_{\mathrm{tot}}(\mathrm{Ni+C})$ and $E_{\mathrm{tot}}(\mathrm{Ni})$ were calculated using the same set of **k** points, FFT grids, etc. μ_{C} was estimated by

TABLE II. Comparison of paramagnetic (ΔH_{sol}^{PM}) and ferromagnetic (ΔH_{sol}^{FM}) heats of solution (in units of eV) calculated for different C sites, using different pseudopotentials (PP), supercell sizes (No. atoms, N_{at}), **k**-point samplings, and exchange-correlation (XC) functionals.

Site	PP	**k**-points	XC	N_{at}	ΔH_{sol}^{PM}	ΔH_{sol}^{FM}
O	US	10	GGA	33	0.19	0.76
O	US	20	GGA	33	0.18	
O	US	10	GGA	65	0.20	
O	PAW	10	GGA	33	0.27	0.71
O	US	10	LDA	33	0.19	0.59
O	PAW	10	LDA	33	0.35	0.75
T	US	10	GGA	33	1.78	2.29
Experiment					0.42, [a] 0.44, [b] 0.49 [c]	

[a]Reference 4.
[b]Reference 3.
[c]Reference 5.

subtracting the heat of formation of graphite (0.025 eV/atom) (Ref. 31) from the energy per atom of diamond obtained from a geometry-optimized primitive cell calculation taken to absolute convergence in total energy[39] ($\sim$1 meV/atom in planewave cutoff and **k**-point sampling).

The calculated heats of solution and available high-temperature experimental data are reported in Table II. Included in the table are results obtained using different exchange-correlation functionals, pseudopotentials, and spin states. Using the US pp set and GGA exchange correlation, we first examined the relative energetics of C placed at the *O* and *T* sites. We find that the paramagnetic ΔH_{sol} at the *O* site of 0.19 eV is 1.59 eV lower in energy than at the *T* site, making the *O* site the preferred C position (in the FM state the difference in energy between sites is similar). The positive sign of ΔH_{sol} indicates that the dissolution of C from graphite into Ni as a solid solution is an endothermic process. The *O* site is preferred because it minimizes local lattice strain; interstitial atoms generally produce distortions within the surrounding lattice, and the *O* site, having the larger amount of free volume, is most able to accommodate the C atom while minimizing this strain. This aspect can be quantified by comparing the formation volumes V^F of a C interstitial at each site

$$V^F = V(\mathrm{Ni+C}) - 32\Omega_0(\mathrm{Ni}), \tag{2}$$

here V(Ni+C) is the relaxed Ni+C supercell volume and Ω_0(Ni) is the volume per atom of elemental Ni. For the *O* site we find $V^F(O\ \mathrm{site}) = 0.80\Omega_0$ ($0.64\Omega_0$) in the PM (FM) state. The *T* site exhibits a larger formation volume $V^F(T\ \mathrm{site}) = 0.97\Omega_0$ ($0.92\Omega_0$) in the PM (FM) state. The relaxed Ni-C bond lengths at the *O* site (*T* site) are 1.85 (1.75 Å).

A charge density difference contour plot ($\Delta\rho$) showing the redistribution of charge for C at an *O*-site relative to the isolated C atomic charge density and the Ni bulk charge density is shown in Fig 1. Consistent with its larger electronegativity, there is a net transfer of charge to the C, apparently arising from the depletion of adjacent Ni d_{z^2} orbitals, indicating an ionic interaction. In addition, there is accumulation of charge along the C-Ni bond lines. This could represent additional partially covalent bonding or simply be a consequence of the symmetry of the Ni-C ionic bond. (A more detailed assessment of the Ni-C bonding interaction would require evaluation of mulliken populations, and has not been performed here.)

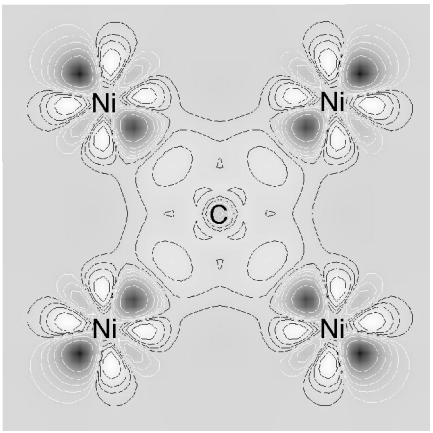

FIG. 1. Charge density difference plot [$\Delta\rho = \rho$(Ni+C) $-\rho$(Ni bulk) $-\rho$(C)] for C in an *O* site showing four of the six nearest-neighbor Ni atoms. Black (white) contours and white (black) shading indicate charge accumulation (depletion), relative to the sum of the isolated C atomic charge density and the bulk Ni charge density. Accumulation contours are drawn at 0.015, 0.05, 0.1, and 0.2 electrons/Å^3; depletion contours are shown for -0.02, -0.05, -0.1, -0.2, -0.4 electrons/Å^3.

Experimental high-temperature ($T > T_c$) measurements of C solubility in Ni have reported ΔH_{sol} values in the range of 0.42–0.49 eV.[3–5] Assuming that the relevant spin state for comparing to these temperatures is the PM state, the first of our ΔH_{sol} calculations using the GGA and US pp's gave $\Delta H_{sol} \approx 0.2$ eV. Although agreement with experiment to about 0.2 eV is reasonable, and earlier calculations[28,29] of ΔH_{sol} for Si in Al have reported similar underestimates with respect to experiment, we briefly examined whether use of a different set of computational parameters would improve agreement with experiment.

One explanation for the underestimate could be related to numerical difficulties in evaluating Eq. (1), which requires a difference between energies of subsystems calculated with different parameters. Secondly, our calculations do not account for finite-temperature thermodynamic effects such as lattice vibrations.[32,33] Other possibilities include difficulties with the exchange-correlation functionals or the pseudopotential approximation. To assess these latter issues we performed additional ΔH_{sol} calculations with the LDA and the PAW pp set; the results of these tests are listed in Table II. Examining the US pp's first, we find no difference between LDA and GGA calculations: Both give $\Delta H_{sol} = 0.19$ eV. However, switching to the PAW pp's gives a definite improvement over the US pp's: The PAW LDA ΔH_{sol} value of 0.35 eV is in the best agreement with experiment, while the PAW GGA predicts $\Delta H_{sol} = 0.27$ eV. The apparent superior

accuracy of the PAW pp sets is likely a reflection of their more realistic representation of the valence wavefunctions within the core region. Especially in the case of interstitial solid solutions, where the interatomic distance between solute and solvent can be quite small, an accurate description of the core region is advantageous. The fact that the LDA PAW ΔH_{sol} value is the largest overall is at least partially due to the LDA's underestimation of bulk lattice constants (see Table I), resulting in less free volume at the interstitial sites.

As mentioned earlier, experiments on the Ni-H (Ref. 6) and NiCo-C (Ref. 7) systems have found an abrupt increase in ΔH_{sol} upon passing below T_c; for Ni-H the change has been estimated to be about 0.1 eV. Here we briefly examine whether such an effect is observable within DFT for the Ni-C system by comparing ΔH_{sol} values obtained with Ni in the ferromagnetic and paramagnetic states. A more complete explanation of this effect is presented elsewhere.[8]

Table II shows that, regardless of pp choice or exchange-correlation functional, the calculated ΔH_{sol} in the ferromagnetic Ni state is about 0.4–0.5 eV larger than in the paramagnetic state. By partitioning the spin-polarized charge into atom-centered Wigner-Seitz spheres, it is possible to obtain semiquantitative information regarding the impact of the octahedral C interstitial on the Ni magnetic moments. We find that the moments on the six nearest-neighbor Ni atoms are partially quenched to about $0.2\mu_B$; the moments of more distant neighbor shells are largely undisturbed. (The C atom does not exhibit a magnetic moment.) Since the demagnetization of the Ni is energetically unfavorable, it is likely to be at least partially responsible for the FM increase in ΔH_{sol}. The cost in magnetization energy to reduce the magnetic moment of a Ni atom from $0.6\mu_B$ to $0.2\mu_B$ is about 45 meV for the PAW pp within the GGA. We note that multiplying this number by 6 (accounting for the octahedral coordination) gives 0.27 eV, which accounts for only about half of the calculated ΔH_{sol} increase. Thus it appears that the increased ΔH_{sol} is not solely due to demagnetization of nearest-neighbor Ni.

The fact that experimentally observed changes in ΔH_{sol} occur at the Curie point in the related NiCo-C and Ni-H systems suggests that our results predicting a change in Ni-C ΔH_{sol} at T_c are reasonable. However, solubility experiments on Ni-C have not been conducted for $T<T_c$, presumably because Ni has a relatively low Curie temperature resulting in very slow kinetics. Therefore, we cannot currently assess whether the magnitude of the predicted ΔH_{sol} change is accurate, and this issue is left as a challenge to experiment.

IV. C CLUSTERING

In a recent experiment, Numakura and co-workers[1] measured the internal friction peak (at 520 K) due to anelastic relaxation of associated C pairs in Ni as a function of C concentration (Fig. 2). Based on the slope of the peak magnitude vs C concentration, they determined that the binding energy (B) between C atoms was small, and probably less than 0.1 eV. Using the mass-action law for the reaction C+C→C-C (pair), they proceeded to estimate the overall concentration of C pairs

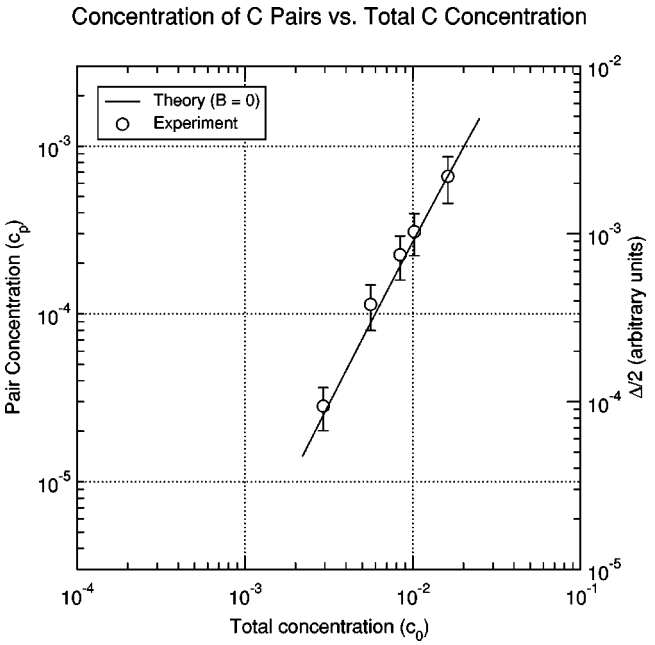

FIG. 2. The magnitude of the relaxation peak ($\Delta/2$) measured at 520 K due to C-C pairs in Ni, adapted from Numakura and co-workers[1] (data points, right ordinate), compared to the present *ab initio* calculations of C pair concentration vs total C concentration (solid line, left ordinate).

$$\frac{c_p}{(c_0-2c_p)^2}=\frac{z}{2}\exp\frac{B}{k_BT}, \tag{3}$$

where c_0 is the total C concentration, z is the coordination number (assuming an octahedral interstitial site, $z=6$), and T is the absolute temperature. To analyze their results, we have calculated the C-C binding energy directly for two different C pair configurations relative to isolated C atoms.

Our clustering calculations used a large Ni supercell constructed from a $3\times3\times3$ replication of the conventional unit cell, resulting in a total of 108 Ni atoms, and a C concentration of 1.8%. A supercell of this size is desirable so as to minimize image-image interactions and to attain a C concentration close to the 1% level used in experiment.[1] A **k**-point convergence test found that four irreducible **k** points were sufficient to converge the total energy of the isolated C atom configuration to within 10 meV. Since energy differences converge faster than total energies, this level of precision

TABLE III. GGA binding energies B (in eV) of C pairs with respect to isolated C atoms at nearest-neighbor (NN) and next-nearest-neighbor (NNN) octahedral sites. Isolated configurations are assigned $B=0$, and configurations with $B<0$ indicate a repulsive C-C interaction.

		C configuration		
PP	Spin state	NN	NNN	Isolated
US	PM	−0.27	−0.20	0
US	FM	−0.07	−0.05	0
PAW	PM	−0.19	−0.15	0
PAW	FM	0.01	−0.01	0

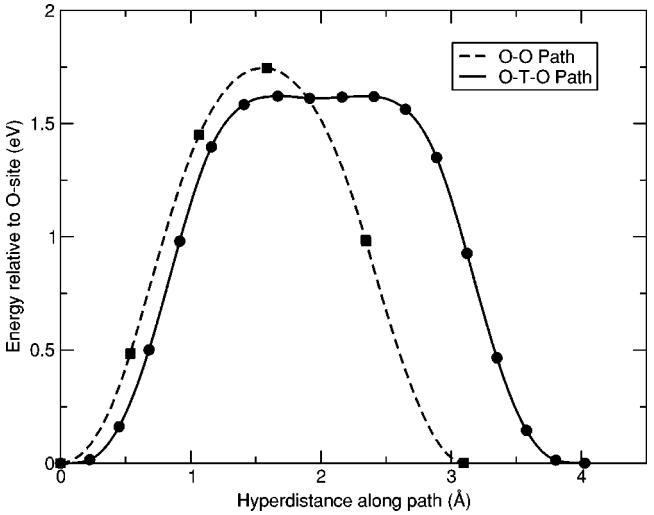

FIG. 3. Activation energy for C interstitial diffusion between *O* sites via two different pathways.

was deemed sufficient. Two C atoms were placed in each supercell in one of three different configurations: isolated octahedral interstitial sites (with the C's separated along the cell's body diagonal in order to maximize the distance between them), nearest-neighbor octahedral sites, and next-nearest-neighbor octahedral sites. As done in the heat-of-solution calculations, both the supercell lattice constant and internal atomic coordinates were optimized.

The C-C pair binding energies obtained from our calculations are reported in Table III. Included in the table are data comparing both ferromagnetic and paramagnetic spin states, and US with PAW pp's. Here we did not examine exchange-correlation functionals, and report only GGA values. Both pp sets predict a repulsive C-C interaction in the paramagnetic state of roughly -0.2 eV for both pair configurations, indicating that isolated interstitials are preferred at high temperatures. Conversely, the ferromagnetic calculations predict a weaker, almost negligible, C-C interaction, with $B \approx 0$ for the (presumably) more accurate PAW pp set, consistent with Numakura's estimate[1] of $B < 0.1$ eV for $T < T_c$. Taking $B = 0$ in equation Eq. (2), and setting $T = 520$ K, we compare our calculated concentration of C pairs with the data obtained by internal friction measurements[1] in Fig. 2. We again find good agreement.

The difference in clustering behavior between the PM and FM states can be explained in terms of a competition between strain effects and magnetic quenching. In the paramagnetic state, the primary interaction between interstitials is via their strain fields, which is repulsive, resulting in a (negative) binding energy of about -0.2 eV. However, in the ferromagnetic state, corresponding to the conditions under which Numakura *et al.* conducted their experiments, the solute atoms partially quench the local moments of neighboring Ni atoms[8] and therefore further raise the total energy of the system. Clustering of the interstitials minimizes the disruption to the Ni's magnetism relative to when the C's are isolated, resulting in a smaller overall energy penalty. In fact, the energy savings achieved in minimizing the magnetic disruption due to clustering roughly cancels the energy cost associated with the lattice strain about an interstitial, resulting in a binding energy of approximately zero in the FM state.

V. C DIFFUSION

To estimate the activation energy (E_a) for C interstitial diffusion between *O* sites, we utilized the optimized 33-atom Ni supercell geometry determined in the *O*-site ΔH_{sol} calculations combined with identical settings for **k**-point sampling, FFT grids, and cutoff energy. The barrier height and associated minimum energy pathway were evaluated using the nudged elastic band method (NEB) of Jónsson and co-workers.[34–36] In this method a series of system images span the hyperdistance between predefined, stationary local minima on the potential energy surface. The minimum energy path between endpoints is then determined by minimizing the forces on each image normal to the local hypertangent between them. (In the present study the forces are minimized using the ''quick-min'' algorithm[37] to a tolerance of 0.05 eV/Å.) This approach prevents so-called corner-cutting and image agglomeration;[34] furthermore, the forces projected along the hypertangent at each image (i.e., the derivative of the energy vs. hyperdistance) can be used to refine the estimate of E_a through spline interpolation.

Using relaxed *O*-sites as the endpoints [see Fig. 4(a)], combined (initially) with the US pp's and GGA exchange correlation, we investigated two different pathways assuming the paramagnetic spin state. The first pathway (the *O*-*O* path), being the one that minimizes the distance between *O* sites, involves translating the C atom directly through the left edge of the starting octahedron. This path used four images, and results in a E_a at the saddle point of 1.75 eV (see Fig. 3), occurring—not surprisingly—as the C squeezes past the two Ni atoms at the vertices of the octahedron's edge. However, our second NEB calculation (using 16 images) revealed that passing instead through an adjacent *T* site via a face of

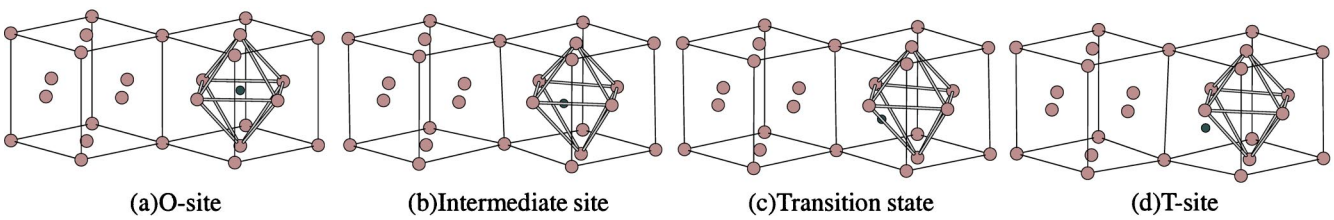

FIG. 4. The first half of the interstitial *O*-*T*-*O* diffusion pathway. Gray (black) spheres represent Ni (C) atoms. Gray bonds representing octahedral structure of the starting configuration (panel a) have been added, and for clarity only a portion of the 33-atom supercell is shown.

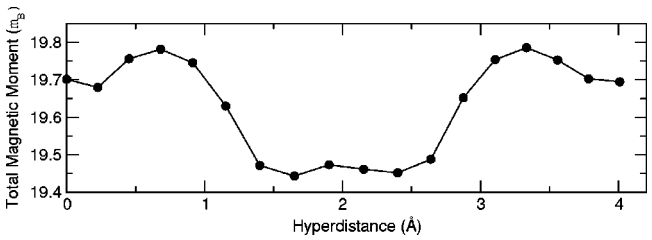

FIG. 5. Total magnetic moment of the Ni+C supercell as a function of NEB image for the *O-T-O* diffusion path. See Fig. 3 for the corresponding energy profile.

the octahedron (the *O-T-O* path) lowers E_a by 0.13 eV, resulting in a barrier of 1.62 eV. The first half of this mechanism is illustrated in Fig. 4. The energy profile vs hyperdistance is shown in Fig. 3; the shallow local minimum at the midpoint of the path corresponds to the *T* site [Fig. 4(d)], with small maxima, corresponding to the transition states, on either side [Fig. 4(c)]. While E_a for both pathways agree reasonably well with the high-temperature experimental values of 1.54–1.71 eV,[4,9,10,12] we believe that the indirect *O-T-O* mechanism is more likely since its E_a is smaller and slightly closer to experiment.

As mentioned above, internal friction experiments on the Ni-C system conducted by Diamond and Wert[11] both above and below T_c found that the magnetic state of Ni had a negligibly small effect upon E_a. To confirm their result we also calculated the ferromagnetic energy barriers for both pathways, again using the GGA and US pp's. We find that E_a changes, at most, by only 0.02 eV for each pathway relative to the paramagnetic state, in agreement with their findings. The relative independence of E_a upon the magnetic state is consistent with the very small change we observe in the total magnetic moment of the Ni+C supercell as a function of the C reaction coordinate. For example, along the *O-T-O* path the total moment is generally constant throughout the C migration, and decreases only about $0.25\mu_B$ (roughly 1%) upon approaching the saddle point (see Fig. 5). Based on the magnetization energy of Ni, a change in magnetism of this size is consistent with the small, almost negligible, (20 meV) change in E_a.

Lastly, we also briefly compared the *O-O* E_a value calculated above (which used the GGA and US pp's) with that obtained using PAW pseudopotentials and within the LDA. We find that the GGA, PAW E_a of 1.76 eV is nearly identical to the GGA, US value of 1.75 eV, which is somewhat surprising considering that these pp's yielded slightly different ΔH_{sol} values. For the US, LDA combination we find a larger E_a of 1.97 eV, which is reasonable considering the equilibrium LDA Ni lattice constant is about 3% smaller than that predicted by the GGA. Repeating the LDA NEB calculation at the GGA lattice constant gave a barrier of 1.69 eV, which is in better agreement with the GGA value.

VI. CONCLUSIONS

We have performed a density-functional study of the solubility, diffusion, and clustering of C in FCC Ni, aimed at confirming the known experimental data, resolving some outstanding issues, and assessing the accuracy of several aspects of our simulation methodology. In general, we find good agreement between experiment and our calculated values. The preferred C interstitial site is the octahedral site, and diffusion between these sites proceeds via an indirect pathway passing through the tetrahedral site. The magnitude of the energy barrier (E_a) for diffusion (theory: 1.62 eV, experiment: 1.54–1.71 eV) and its insensitivity to the magnetic state of the Ni are consistent with experiment. C-C clusters in the ferromagnetic state were found to have a negligible binding energy (*B*) due to a cancellation between repulsive lattice strain effects and attractive magnetic quenching interactions; at high temperatures the C-C interaction should be repulsive. Our results are in agreement with anelastic relaxation experiments which predict $B<0.1$ eV for $T<T_c$. Our calculated heat of solution (ΔH_{sol}) in the Ni paramagnetic state falls within the range 0.19–0.35 eV depending upon which pp or exchange-correlation functional was implemented. This is in reasonable agreement with, but slightly below, the experimental values of 0.42–0.49 eV. A large increase in ΔH_{sol} of ~ 0.4 eV is observed in the ferromagnetic state, which is consistent with experimentally observed changes in ΔH_{sol} at T_c in the related Ni-H and NiCo-C systems.

Regarding pseudopotentials (pp), in our tests involving ΔH_{sol}, E_a, and *B*, the values predicted by the US pp's were, with one exception, within 0.1 eV of the PAW values. Given their relatively modest requirements for planewave cutoff energy, we conclude that the accuracy of the US pp set is adequate for large-scale simulations involving large supercells and/or complicated diffusion pathways utilizing many nudged elastic band images. Differences due to exchange-correlation functionals (LDA vs GGA) were also examined in calculations of ΔH_{sol} and E_a. In the case of ΔH_{sol} LDA and GGA values differed by less than 0.1 eV; for E_a, when using the respective calculated lattice constant of Ni, the GGA value was in best agreement with experiment. The LDA value was ~ 0.2 eV larger, which was attributed to the LDA's 3% underestimate of the Ni lattice constant.

ACKNOWLEDGMENTS

This work was supported by the U.S. Department of Energy, Office of Basic Energy Sciences, Division of Materials Sciences, under Contract No. DE-AC04-94AL85000.

*Electronic address: djsiege@sandia.gov

[1] H. Numakura, K. Kashiwazaki, H. Yokoyama, and M. Koiwa, J. Alloys Compd. **310**, 344 (2000).

[2] T.E. Buchheit, D. LaVan, J.R. Michael, T.R. Christenson, and S.D. Leith, Metall. Mater. Trans. A **33**, 539 (2002).

[3] K. Natesan and T.F. Kassner, Metall. Trans. **4**, 2557 (1973).

[4] J.J. Lander, H.E. Kern, and A.L. Beach, J. Appl. Phys. **23**, 1305 (1952).

[5] W.W. Dunn, R.B. McLellan, and W.A. Oates, Trans. Metall. Soc. AIME **242**, 2129 (1968).
[6] K. Zeng, T. Klassen, W. Oelerich, and R. Bormann, J. Alloys Compd. **283**, 151 (1999).
[7] M. Hasebe, H. Ohtani, and T. Nishizawa, Metall. Trans. A **16**, 913 (1985).
[8] D.J. Siegel, M. van Schilfgaarde, and J.C. Hamilton (unpublished).
[9] J. Cermak and H. Mehrer, Acta Metall. Mater. **42**, 1345 (1994).
[10] R.P. Smith, Trans. Metall. Soc. AIME **236**, 1224 (1966).
[11] S. Diamond and C. Wert, Trans. Metall. Soc. AIME **239**, 705 (1967).
[12] H. Lafitau, P. Gendrel, and L. Jacque, Compt. Rend. **263C**, 1033 (1966).
[13] P. Hohenberg and W. Kohn, Phys. Rev. **136**, B864 (1964).
[14] W. Kohn and L.J. Sham, Phys. Rev. **140**, A1133 (1965).
[15] G. Kresse and J. Furthmüller, Phys. Rev. B **54**, 11 169 (1996).
[16] D. Vanderbilt, Phys. Rev. B **41**, 7892 (1990).
[17] G. Kresse and J. Hafner, J. Phys.: Condens. Matter **6**, 8245 (1994).
[18] G. Kresse and D. Joubert, Phys. Rev. B **59**, 1758 (1999).
[19] H.J. Monkhorst and J.D. Pack, Phys. Rev. B **13**, 5188 (1976).
[20] M. Methfessel and A.T. Paxton, Phys. Rev. B **40**, 3616 (1989).
[21] J.P. Perdew, J.A. Chevary, S.H. Vosko, K.A. Jackson, M.R. Pederson, D.J. Singh, and C. Fiolhais, Phys. Rev. B **46**, 6671 (1992).
[22] D.M. Ceperley and B.J. Alder, Phys. Rev. Lett. **45**, 566 (1980).
[23] J.P. Perdew and A. Zunger, Phys. Rev. B **23**, 5048 (1981).
[24] P.E. Blöchl, Phys. Rev. B **50**, 17 953 (1994).
[25] J. Cho and M. Scheffler, Phys. Rev. B **53**, 10 685 (1996).
[26] H.C. Herper, E. Hoffmann, and P. Entel, J. Phys. IV **7**, 71 (1997).
[27] C. Kittel, *Introduction to Solid State Physics*, 6th ed. (John Wiley and Sons, New York, 1986).
[28] N. Chetty, M. Weinert, T.S. Rahman, and J.W. Davenport, Phys. Rev. B **52**, 6313 (1995).
[29] D.E. Turner, Z.Z. Zhu, C.T. Chan, and K.M. Ho, Phys. Rev. B **55**, 13 842 (1997).
[30] F.D. Murnaghan, Proc. Natl. Acad. Sci. U.S.A. **30**, 244 (1944).
[31] R.C. Weast, ed., *CRC Handbook of Chemistry and Physics*, 67th ed. (CRC Press, Boca Raton, FL, 1983).
[32] A. van de Walle and G. Cedar, Rev. Mod. Phys. **74**, 11 (2002).
[33] V. Ozolins and M. Asta, Phys. Rev. Lett. **86**, 448 (2000).
[34] H. Jónsson, G. Mills, and K. W. Jacobsen, *Classical and Quantum Dynamics in Condensed Phase Simulations* (World Scientific, Singapore, 1998), p. 385.
[35] G. Henkelman, B.P. Uberuaga, and H. Jónsson, J. Chem. Phys. **113**, 9901 (2000).
[36] G. Henkelman and H. Jónsson, J. Chem. Phys. **113**, 9978 (2000).
[37] G. Henkelman and H. Jónsson, J. Chem. Phys. **111**, 7010 (1999).
[38] L.A. Girifalco and M. Hodak, Phys. Rev. B **65**, 125404 (2002).
[39] It is well-known (Ref. 38) that DFT does not properly account for dispersion forces, such as those between graphene sheets in graphite. Hence, our reference for the energy/atom of graphite uses the diamond atomic energy minus the formation energy difference between the two phases. Using the US C pp, in conjunction with 35 **k** points and a cutoff energy of 290 eV, our calculations on bulk diamond gave good agreement with experiment. For example, lattice constant: 3.57 Å calculated, 3.57 Å experiment (Ref. 27); bulk modulus: 431 GPa calculated, 443 Å experiment. Equivalent accuracy was obtained with the PAW pp's.